

Stereochemical effects on intervalence charge transfer*

Deanna M. D'Alessandro[‡] and F. Richard Keene

School of Pharmacy and Molecular Sciences, James Cook University, Queensland 4811, Australia

Abstract: Recent work has revealed the first observation of stereochemical effects on intervalence charge transfer (IVCT) in di- and trinuclear mixed-valence complexes. The differential IVCT characteristics of the diastereoisomers of polypyridyl complexes of ruthenium and osmium offer a new and intimate probe of the fundamental factors that govern the extent of electronic delocalization and the barrier to electron transfer. These findings challenge prior assertions that the inherent stereochemical identity of such complexes would have no influence on the intramolecular electron-transfer properties of polymetallic assemblies. This article provides a brief review of the past 40 years of mixed-valence research and looks at recent progress in stereochemical effects on IVCT. The implications of the findings are considered within the context of the existing theoretical and experimental framework for IVCT.

Keywords: mixed valence; electron transfer; dinuclear; stereochemistry; intervalence charge transfer.

BACKGROUND AND SCOPE

The fundamental importance of electron transfer underlies the extensive multidisciplinary research efforts which have led to the discovery of mixed-valence complexes, a class of transition-metal-based compounds which contain ions of the same element in different formal oxidation states. The significance of the mixed-valence phenomenon was elucidated in the early 20th century with the realization that the valences are in rapid oscillation between the metal centers (rather than being uniquely fixed, one to each ion) [1,2], giving rise to the absorption of light in the visible region of the electromagnetic spectrum.

Four decades have now passed since the first efforts to understand mixed valency, and a recent Royal Society meeting on Mixed Valency in Chemistry, Physics and Biology in March 2007 was dedicated to the pioneering scientists in the field. This article provides an overview of the rich history of mixed-valence research and discusses the recent discovery of stereochemical effects in mixed-valence complexes.

Mixed valency in chemistry, physics, and biology

The first synthetic mixed-valence compound, “Prussian blue”, $\text{Fe}^{\text{II}}\text{Fe}^{\text{III}}(\text{CN})_6 \cdot x\text{H}_2\text{O}$, has been prized industrially for centuries as an ink and dye-stuff. This infinite three-dimensional cubic array of alternate Fe^{II} and Fe^{III} centers linked by bridging cyanide (CN^-) groups exhibits an intense blue coloration which cannot be attributed to a combination of the individual absorption spectra of the constituent ions [2].

Pure Appl. Chem.* **80, 1–57 (2008). A collection of invited, peer-reviewed articles by the winners of the 2007 IUPAC Prize for Young Chemists.

[‡]Corresponding author

The mixed-valence nature of the species gives rise to an intervalence charge transfer (IVCT) transition between the metal centers which corresponds to the absorption of light in the visible region of the spectrum.

The reaction centers in bacterial, algal, and plant systems constitute elaborate examples of biological mixed-valence systems. In the natural photosynthetic process, the primary electron donor is the "special-pair", P—a membrane-bound protein comprising two bacteriochlorophyll molecules. Photoexcitation of the reaction center gives rise to a long-lived, charge-separated state, and the resultant special-pair radical cation P^+ is a mixed-valence species [3].

The elegance and efficiency of the charge separation function in photosynthetic organisms has provided the inspiration for the design and synthesis of many ingenious model systems [4,5]. Polypyridyl complexes of the d^6 metals ruthenium(II) and osmium(II) have been extensively employed as the basis for such systems due to their unique combination of photochemical, photophysical, and redox properties, including the stability of their ground and excited states, and their chemical inertness in a variety of oxidation states [6].

Dinuclear mixed-valence complexes of ruthenium and osmium provide ideal model systems for elucidating the fundamental factors that govern intermolecular electron-transfer reactions in natural and artificial systems. In the late 1960s, Allen and Hush [1] and Robin and Day [2] published seminal reviews of mixed-valence materials. Hush subsequently provided a theoretical model linking the physical properties of dinuclear mixed-valence complexes (i.e., the parameters of their IVCT absorption bands) to the activation barriers for electron transfer from Marcus theory [7,8]. Of particular significance was the prediction of a relationship between the energy of the intervalence transition (ν_{\max}) and several factors which govern the activation barrier:

$$\nu_{\max} = h\nu = \lambda_i + \lambda_o + \Delta E_0 + \Delta E' \quad (1)$$

The Franck–Condon factors, λ_i and λ_o , correspond to the reorganizational energies within the inner- and outer-sphere (respectively), the redox asymmetry, ΔE_0 , is the thermodynamic energy difference between the two metal-based chromophores, and $\Delta E'$ reflects any additional energy contributions due to spin-orbit coupling and ligand field asymmetry. To date, these factors have been probed by varying the "global" features of dinuclear complexes such as the identity and coordination environments of their constituent metal centers, or through the introduction of redox asymmetry. The reorganizational energy contributions are typically assessed by varying the macroscopic features of the external environment such as the solvent, anions, and temperature.

Recent work in our laboratory has involved the first investigation of IVCT in stereochemically pure di- and trinuclear polypyridyl complexes of ruthenium and osmium. The *subtle* and *systematic* variations in the geometries of the stereoisomers have been shown to provide a new experimental probe for the factors which govern the barriers to electron transfer at the molecular level.

Theoretical background: IVCT in dinuclear mixed-valence complexes

The IVCT transition in dinuclear mixed-valence species may be examined by considering a complex of the type $\{[Ru_1(L)_n](\mu-BL)[Ru_2(L)_n]\}^{4+}$ (where L and BL represent the terminal and bridging ligands, respectively), hereafter abbreviated $[Ru_1^{II}Ru_2^{II}]$, where both metal centers are in the +2 oxidation state. The oxidation of one ruthenium center gives rise to the mixed-valence species $[Ru_1^{II}Ru_2^{III}]$, where the overall +5 charge corresponds to $[Ru_1^{II}Ru_2^{III}]$ in a fully localized description and $[Ru_1^{II1/2} Ru_2^{III1/2}]$ in a fully delocalized description [7,8].

The optically induced IVCT transition (eq. 2) corresponds to the formation of the vibrationally excited state of the ion, $[Ru_1^{III}Ru_2^{II}]^*$. Since this process proceeds faster than nuclear motion (in accordance with the Franck–Condon principle), $[Ru_1^{III}Ru_2^{II}]^*$ contains $[Ru_1^{III}]^*$ in a coordination environment appropriate for $[Ru_1^{II}]_0$, and $[Ru_2^{II}]^*$ in a coordination environment appropriate for $[Ru_2^{III}]_0$.



Four decades have passed since Robin and Day [2] published their seminal paper in 1967 classifying mixed-valence systems based on the strength of their metal-metal coupling into three classes. In that same year, Hush published his pioneering theoretical model linking the physical properties of dinuclear mixed-valence complexes to the activation barriers for electron transfer from Marcus theory [7,8].

IVCT measurements on dinuclear complexes provide a sensitive and powerful probe to elucidate aspects of intramolecular electron-transfer processes. The energies (ν_{max}), intensities (ϵ_{max}), and bandwidths at half-height ($\Delta\nu_{1/2}$) of the absorption bands may be quantitatively related to the factors which influence the barrier to intramolecular electron transfer according to the classical theory developed by Hush [7,8].

In accordance with the Robin and Day [2] classification scheme, in class I systems, the interaction between the metal centers is negligible and IVCT transitions are not possible. Class II systems are characterized by weak to moderate electronic coupling between the metal centers, and generally exhibit broad, solvent-dependent, Gaussian-shaped IVCT bands ($\epsilon_{\text{max}} \leq 5000 \text{ M}^{-1} \text{ cm}^{-1}$, $\Delta\nu_{1/2} \geq 2000 \text{ cm}^{-1}$). The strong electronic coupling in class III systems gives rise to narrow, solvent-independent, and high-intensity IVCT bands ($\epsilon_{\text{max}} > 5000 \text{ M}^{-1} \text{ cm}^{-1}$, $\Delta\nu_{1/2} < 2000 \text{ cm}^{-1}$).

For Gaussian-shaped IVCT bands, the predicted bandwidth at half-height is $\Delta\nu_{1/2}^\circ = [16RT\ln 2(\nu_{\text{max}} - \Delta E_0 - \Delta E')^{1/2}]^{1/2}$, where R is the gas constant, T is the temperature (in K), and the term $16RT\ln 2$ takes a value of 2310 cm^{-1} at 298 K [7,8].

The degree of electronic coupling is generally quantified by the electronic coupling matrix element, H_{ab} (eq. 3) [7,8], where r_{ab} is the distance between the two metal centers. A more rigorous quantum mechanical formulation is given by eq. 4 [9,10], where $|\mu_{12}|$ is the adiabatic transition dipole moment and e is the unit electronic charge. This form of the equation for H_{ab} has the advantage that no implicit assumption is made regarding the shape of the IVCT band, as $|\mu_{12}|$ may be calculated from the integrated intensity of the band [10].

$$H_{\text{ab}} = \frac{2.06 \times 10^{-2} (\nu_{\text{max}} \epsilon_{\text{max}} \Delta\nu_{1/2})^{1/2}}{r_{\text{ab}}} \quad (3)$$

$$H_{\text{ab}} = \frac{|\mu_{12}|}{er_{\text{ab}}} \nu_{\text{max}} \quad (4)$$

According to the Robin and Day classification scheme [2], the above-mentioned classes of mixed-valence systems are distinguished by the relative magnitudes of λ ($= \lambda_i + \lambda_o$) and $2H_{\text{ab}}$. For weakly coupled class II systems, $2H_{\text{ab}} \ll \lambda$. When Ru_1 and Ru_2 are strongly electronically coupled ($2H_{\text{ab}} \gg \lambda$), the thermal barrier to intramolecular electron transfer vanishes and both metal centers possess a partial oxidation state of +2.5. In this case, the IVCT transitions occur within the molecular orbital manifolds of the systems and the energies of the IVCT bands provide a direct measure of H_{ab} according to $\nu_{\text{max}} = 2H_{\text{ab}}$ [7,8].

Reorganizational energy contribution

Classically, the reorganizational energy is composed of an inner-sphere vibrational component, λ_i , corresponding to the energy required for reorganization of the metal–ligand and intra-ligand bond lengths and angles, and an outer-sphere component, λ_o , corresponding to the energy required for reorganization of solvent and anion molecules in the surrounding medium.

The solvent reorganizational energy (λ_o) is generally modeled as a one-dimensional classical mode due to the low frequencies of the coupled vibrations [7,8,11,12]. The spherical cavity dielectric continuum model given by eq. 5 provides a framework for the calculation of this contribution in which

the electron donor and acceptor are modeled as two non-interpenetrating spheres, embedded in the dielectric continuum [7,8].

$$\lambda_o = e^2 \left(\frac{1}{a} - \frac{1}{d} \right) \left(\frac{1}{D_{op}} - \frac{1}{D_s} \right) \quad (5)$$

The parameters a and d define the molecular radii and distance between the donor and acceptor, e is the unit electronic charge, and D_s and D_{op} are the macroscopic static and optical dielectric constants of the solvent, respectively. In accordance with eqs. 1 and 5, (i) ν_{\max} should vary linearly with the solvent dielectric function $(1/D_{op} - 1/D_s)$, with slope $e^2(1/a - 1/d)$ and intercept $\lambda_i + \Delta E'$ at $(1/D_{op} - 1/D_s) = 0$, and (ii) ν_{\max} should vary linearly with $1/d$, with slope $e^2(1/D_{op} - 1/D_s)$ in a given solvent in which the length of the bridging ligand is varied (at fixed a). The sensitivity of IVCT bands to solvent variation is often employed as a criterion for the class of a mixed-valence species: a solvent dependence signals valence localization (class II), while a solvent independence signals delocalization (class III) [13–15].

Transition between localization and delocalization

A pivotal problem in the analysis of mixed-valence complexes is the extent of electronic delocalization between the metal centers—which is governed by competition between the electronic coupling (H_{ab}) and the sum of the Franck–Condon reorganizational energy, the redox-asymmetry (ΔE_0), and additional contributions due to spin-orbit coupling and ligand field asymmetry ($\Delta E'$) [7,8].

The two-state Hush model [7,8] has provided the preferred method of analysis for mixed-valence complexes, and the validity of the model for the determination of the relative contributions of the fundamental parameters expressed in eq. 1 has been extensively tested and reviewed [13,15–24]. Experimentally, these contributions have been probed by the dependence of the IVCT characteristics on structural and substitutional changes in the mixed-valence systems. These include the distance between the metal centers [16], the ability of the bridging ligand to delocalize the electronic charge [25], and the coordination environment of the metal centers [13,15,17,18,20–22], which can be controlled through variations in the metal centers and the bridging or terminal ligands. The characteristics of the external medium such as the identity of the solvent and anions also constitute critical contributions to the electron-transfer barrier [23]. While the classical two-state model [7,8] has been successfully applied to the analysis of complexes in the strongly localized and delocalized limits, apparent breakdowns occur between these two extremes in the presence of significant electronic delocalization, or specific solvent–solute interactions.

For systems near the localized-to-delocalized transition, the IVCT bands are frequently asymmetrically shaped and intense [20,25,26]. The various theoretical treatments attribute asymmetry to different effects, and previous modeling studies have attempted to reproduce the line-width by several methods [20]. Within the two-state classical model, the asymmetry is a natural consequence of the “band cut-off effect” in which the IVCT band is Gaussian-shaped on the high-energy side, skewed on the low-energy side, and truncated at $\nu \leq 2H_{ab}$ [20,25–27]. Alternatively, there may be contributions from overlapping mixed-valence transitions, differences in the extent of electronic delocalization between the ground and mixed-valence excited states, or contributions from a vibronic progression or progressions [20].

Experimentally, the classification of mixed-valence complexes as localized (class II), delocalized (class III), or intermediate localized-to-delocalized systems is generally based upon the observed bandwidth at half-height ($\Delta\nu_{1/2}$) compared with that calculated [7,8] in the limit of a localized two-site transition ($\Delta\nu_{1/2}^\circ$). A system is localized if $\Delta\nu_{1/2} \geq \Delta\nu_{1/2}^\circ$ and delocalized if $\Delta\nu_{1/2} < \Delta\nu_{1/2}^\circ$. However, the discrimination between the two regimes is not straightforward as band-shape analyses are frequently complicated by multiple overlapping transitions, and a significant number of mixed-valence systems exhibit the characteristics of *both* localized and delocalized systems. Meyer and coworkers [20] ad-

addressed this conundrum by defining systems in the localized-to-delocalized transition as “class II–III”. In reality, the transitions between the classes are not abrupt, and their distinction is based on the relative time-scales of the solvent, vibrational, and electronic motions [20]. The challenging nature of classification is reminiscent of the arguments involved in the study of the Creutz–Taube ion, $[\{\text{Ru}(\text{NH}_3)_5\}_2(\mu\text{-pyz})]^{5+}$ (pyz = pyrazine) [28,29], and its derivatives. Due to the limited number of experimental studies in which the subtleties in behavior in the localized-to-delocalized transition have been systematically explored, there is currently extensive interest in the preparation of systems which exhibit class II–III behavior [19,20,25,26,30]. The stereoisomers of dinuclear mixed-valence complexes offer ideal model systems for such studies.

STEREOCHEMISTRY IN POLYMETALLIC ASSEMBLIES

Polymetallic assemblies which comprise octahedral coordination centers with bidentate ligands exhibit stereoisomerism due to the inherent chirality of the component metal centers. An octahedral metal center with at least two symmetrical bidentate ligands, such as the archetypal tris(bidentate) species $[\text{Ru}(\text{bpy})_3]^{2+}$ (bpy = 2,2'-bipyridine), possesses two chiral forms (known as *enantiomers*), designated Λ (left-handed) and Δ (right-handed). The UV/vis/NIR spectral, electrochemical, and NMR characteristics of the enantiomeric forms are identical in an achiral environment, and differ only when the technique used to probe them is itself chiral, e.g., circular dichroism (CD) spectroscopy.

A homo-dinuclear complex of the form $[\{\text{M}(\text{pp})_2\}_2(\mu\text{-BL})]^{4+}$ constitutes the simplest example of a polymetallic assembly, where pp is a symmetrical bidentate ligand such as bpy, and BL is a symmetrical di-bidentate bridging ligand such as bpm (2,2'-bipyrimidine), as shown in Fig. 1 [31,32].

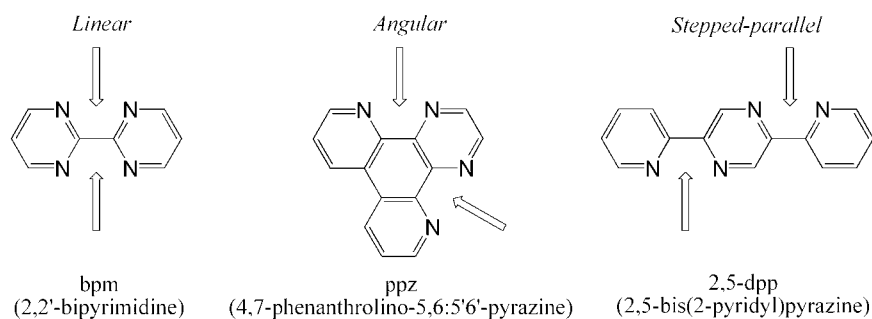


Fig. 1 Examples of bridging di-bidentate ligands commonly used in the construction of polymetallic assemblies. The bridging ligands may be categorized as linear, angular, or stepped-parallel based on the relative disposition of the bidentate coordination sites.

The dinuclear complex $[\{\text{Ru}(\text{bpy})_2\}_2(\mu\text{-bpm})]^{4+}$ may exist in three possible stereoisomeric forms—a *meso* form ($\Delta\Delta \equiv \Lambda\Lambda$; point group symmetry C_{2h}), and a *racemic* (*rac*) form (point group symmetry D_2), which comprises the enantiomeric pair $\Delta\Delta$ and $\Lambda\Lambda$ (Fig. 2a) [31,32]. As shown in Fig. 2b, the relative positions and coordination environments of the metal centers are identical for each diastereoisomer, however, a significant difference may be discerned in the relative orientations of the terminal bpy ligands [31,32]. When the relationship between the axes of the “bites” of the two coordination sites of the bridging ligand are linear (e.g., bpm) or stepped-parallel (e.g., 2,5-dpp), the terminal ligands “above” and “below” the plane of the bridge are approximately parallel in the *rac* ($\Delta\Delta/\Lambda\Lambda$) form and orthogonal in the *meso* ($\Lambda\Delta$) diastereoisomer. However, when the “bites” are angular (e.g., ppz), this description is reversed.

The stereoisomeric complexity of polymetallic assemblies increases with the nuclearity of the system, and in the presence of unsymmetrical bridging or peripheral ligands [31–33]. The development

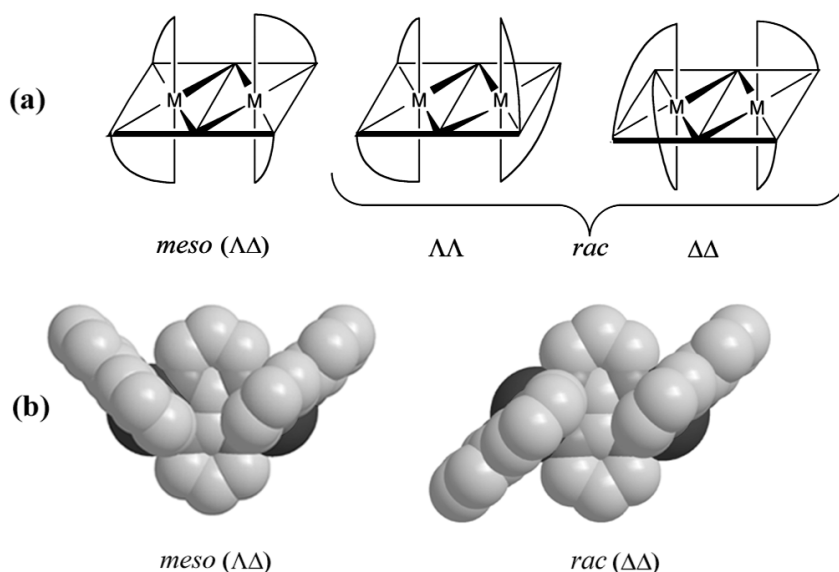


Fig. 2 (a) Schematic representation of the two diastereoisomeric forms of $[M(pp)_2]_2(\mu-BL)^{4+}$ ($M = Ru$ or Os ; pp = a symmetrical bidentate ligand; BL = a linear bridging ligand). (b) Chem3D representations of the *meso* ($\Lambda\Delta$) and *rac* ($\Delta\Delta$) diastereoisomers of $[Ru(bpy)_2]_2(\mu-bpm)^{4+}$. Views from “above” the plane of the bridging ligand. The terminal bpy ligands “below” the plane omitted for clarity.

of general synthetic methodologies using enantiometrically pure “building blocks” and chromatographic techniques [31,32] pioneered by Keene and coworkers have permitted the isolation of the individual stereoisomers (geometric isomers, diastereoisomers, and enantiomers) of mono-, di-, and trinuclear polypyridyl complexes, as well as helicate species.

Stereochemical effects on intramolecular electron transfer

Over the past two decades, polynuclear assemblies incorporating ligands such as those shown in Fig. 1 have been the subject of extensive research efforts due to their potential as the basis of novel molecular materials [34]. However, there has been little recognition of the stereochemical complexities which are inherent in such assemblies, and measurements on their physical properties have often been conducted on stereoisomeric mixtures [31,32]. Keene and coworkers reported the first four examples of differences in the spectral, electrochemical, and photophysical properties of the stereoisomers in mono-, di-, and trinuclear systems [35–38].

STEREOCHEMICAL EFFECTS ON IVCT

Diastereoisomers as probes for reorganizational effects in IVCT

Historically, the Franck–Condon reorganizational contributions to the electron-transfer barrier have been probed by IVCT solvatochromism studies of symmetrical dinuclear mixed-valence complexes, through the treatment of the solvent as a structureless dielectric continuum (eq. 5). While the predictions of the dielectric continuum model have been verified in a number of IVCT solvatochromism studies of mixed-valence complexes [13,15,23], the treatment breaks down when the underlying assumptions of the classical model are invalidated, or in the presence of specific solvent–solute interactions or dielectric saturation effects which often confound experimental solvatochromism studies [23].

Dielectric continuum theory obscures the “molecularity” of the solvent by neglecting the properties of individual solvent molecules, and this underpins the recent theoretical interest toward understanding the molecular basis of reorganizational effects [19,23]. The experimental strategy for extracting information at the molecular level using IVCT solvatochromism studies involves probing the first solvation shell separately from the bulk solution. Dinuclear ruthenium complexes incorporating amine and cyano ligands have been extensively investigated in this regard, due to the existence of strong directional H-bonding and donor–acceptor interactions between the chromophore ligands and individual solvent molecules [23]. These specific solvent interactions coexist with, and often dominate dielectric continuum effects. Correlations have been found between the IVCT solvent shifts and empirical solvent parameters such as the Gutmann donor and acceptor numbers [39]. IVCT solvatochromism studies in solvent mixtures have demonstrated that the solvent reorganizational process occurs predominantly within the first solvation layer, and may be profoundly influenced by the systematic replacement of individual solvent molecules in the immediate vicinity of the mixed-valence chromophore [23].

The subtle variations in the dimensions of the clefts between the diastereoisomers of symmetrical dinuclear complexes offer a new probe for reorganizational contributions to intramolecular electron transfer due to solvent association at the molecular level. λ_i and $\Delta E'$ are expected to be identical for the diastereoisomers of the same complex, so that IVCT solvatochromism studies of the forms permit a direct probe of spatially directed solvent effects on λ_0 .

The IVCT solvatochromism for the diastereoisomeric forms of $[\{\text{Ru}(\text{bpy})_2\}_2(\mu\text{-bpm})]^{5+}$ was investigated in the homologous series of the nitrile solvents acetonitrile (CH_3CN ; AN), propionitrile ($\text{CH}_3\text{CH}_2\text{CN}$; PN), *n*-butyronitrile [$\text{CH}_3(\text{CH}_2)_2\text{CN}$; BN], *iso*-butyronitrile [$(\text{CH}_3)_2\text{HCCN}$; *i*BN], and benzonitrile ($\text{C}_6\text{H}_5\text{CN}$; BzN). The macroscopic properties of the solvents (as defined by the solvent parameter $1/D_{\text{op}} - 1/D_{\text{s}}$) vary over the range 0.5127 (AN) to 0.3897 (BzN), while the subtle variation in the molecular shape, size, and symmetry through the series of aliphatic and aromatic nitriles allows for a detailed analysis of the microscopic origins of the solvent reorganizational energy due to stereochemically directed solvent effects [40].

In accordance with eqs. 1 and 5, the predicted linear trend between ν_{max} and the “solvent parameter” ($1/D_{\text{op}} - 1/D_{\text{s}}$) is evident in all solvents except AN (Fig. 3) [40]. The energy disparity can be attributed to a *specific* solvent effect which is enhanced for the *rac* relative to the *meso* form: the clefts

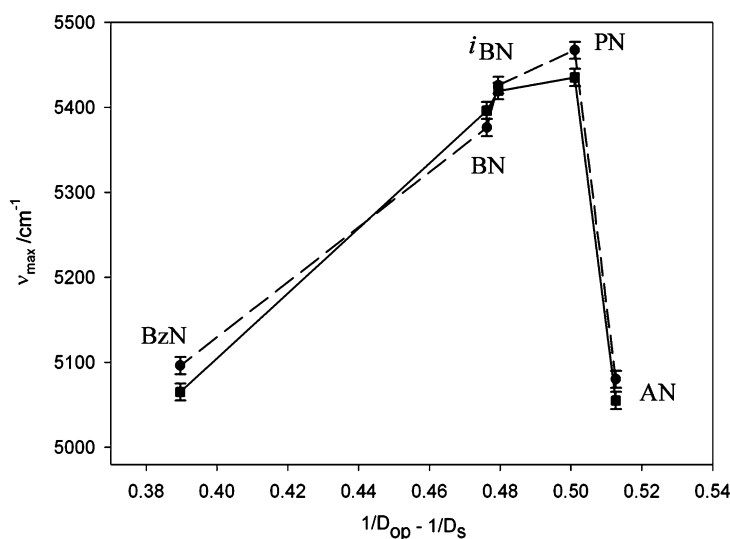


Fig. 3 IVCT solvatochromism for *meso* (solid line) and *rac* (dashed line) $[\{\text{Ru}(\text{bpy})_2\}_2(\mu\text{-bpm})]^{5+}$ in 0.02 M $[(n\text{-C}_4\text{H}_9)_4\text{N}]\{\text{B}(\text{C}_6\text{F}_5)_4\}$ /solvent at +25 °C.

between the terminal bpy rings allow the AN molecules to approach the metal centers more closely than is permitted by dielectric continuum theories of solvation which are typically used to assess the outer-sphere reorganizational energy.

To address the issue of continuum vs. specific solvation, the IVCT characteristics of the diastereoisomeric forms of $[\{\text{Ru}(\text{bpy})_2\}_2(\mu\text{-bpm})]^{5+}$ were investigated as a function of solvent composition in a series of solvent mixtures containing varying mole fractions of AN and PN. The solvent proportion experiments demonstrate that the magnitude of the specific interaction is enhanced for the *rac* relative to the *meso* form, as the dimensionality of the “clefts” between the planes of the terminal polypyridyl ligands are ideally disposed to accommodate discrete solvent molecules [40].

Varying the selectivity of solvent association

Subtle and systematic variations in the sizes and shapes of the clefts through bridging ligand modification and the judicious positioning of alkyl substituents on the terminal ligands reveal that the magnitudes of the effects are dependent on the different cavity dimensions, and the number, size, orientation, and location of solvent dipoles within the clefts.

Increasing the inter-metal distance from 5.6 Å for the bpm-bridged systems to 7.9 Å [41] in the diastereoisomers of $[\{\text{Ru}(\text{bpy})_2\}_2(\mu\text{-dbneil})]^{5+}$ (dbneil = dibenzoeilatin) (at fixed *a*) [40,42] was found to decrease the IVCT solvent dependence. The addition of substituents on the terminal ligands in the series $[\{\text{Ru}(\text{pp})_2\}_2(\mu\text{-bpm})]^{5+}$, where pp = 5,5'-dimethyl-2,2'-bipyridine (5,5'-Me₂bpy), 4,4',5,5'-tetramethyl-2,2'-bipyridine (Me₄bpy), 2,9-dimethyl-1,10-phenanthroline (Me₂phen), and 4,4'-di-*tert*-butyl-2,2'-bipyridine (*t*Bu₂bpy) was also found to dramatically vary the specific solvent effects. For example, bulky *tert*-butyl substituents impede the access of solvent molecules to the clefts leading to negligible IVCT solvatochromism [40].

Quantitatively, the effects cannot be rationalized in terms of existing theoretical solvation models or empirical solvent scales. A more sophisticated molecular solvation model is required, which is parameterized in terms of microscopic solvent properties, including the relative orientation and distance of discrete solvent molecules from the charge-transfer axis. The results summarized here provide an experimental platform which addresses the paucity of experimental data that is available to guide and test developing solvation models which link the dynamics of individual solvent molecules and the Marcus–Hush theory of electron transfer [19,23].

Stereochemical effects on the factors that govern the electron-transfer barrier

The series of complexes $[\{\text{Ru}(\text{bpy})_2\}_2(\mu\text{-BL})]^{4+}$ based on the bridging ligands shown in Fig. 4 have been investigated extensively over the past two decades as the basis of novel molecular materials capable of performing useful light- and/or redox-induced functions [34]. While these studies were performed without regard for the inherent stereochemistry of the systems, stereochemical influences provide a significant contribution to the barrier to intramolecular electron transfer, and are indeed manifested in the electrochemical, spectral, and IVCT properties of the systems.

Our work has detailed the first observation of stereochemical effects on the IVCT transitions in a series of dinuclear polypyridyl complexes of ruthenium and osmium. The systematic variation in the electronic and structural properties of the bridging ligands in the series of complexes $[\{\text{M}(\text{bpy})_2\}_2(\mu\text{-BL})]^{5+}$ (M = Ru, Os) incorporating the linear, angular, and stepped-parallel bridging ligands shown in Fig. 4 has demonstrated the subtle influence of stereochemical and structural factors on the reorganizational energies (λ_o and λ_i), the redox asymmetry (ΔE_0) and the spin-orbit coupling ($\Delta E'$) contributions to the electron-transfer barrier, as expressed in eq. 1. In addition to systematic electronic variations in the series of complexes, the angular or stepped-parallel geometries of the bridging ligands permit subtle changes in the dimensions of the clefts.

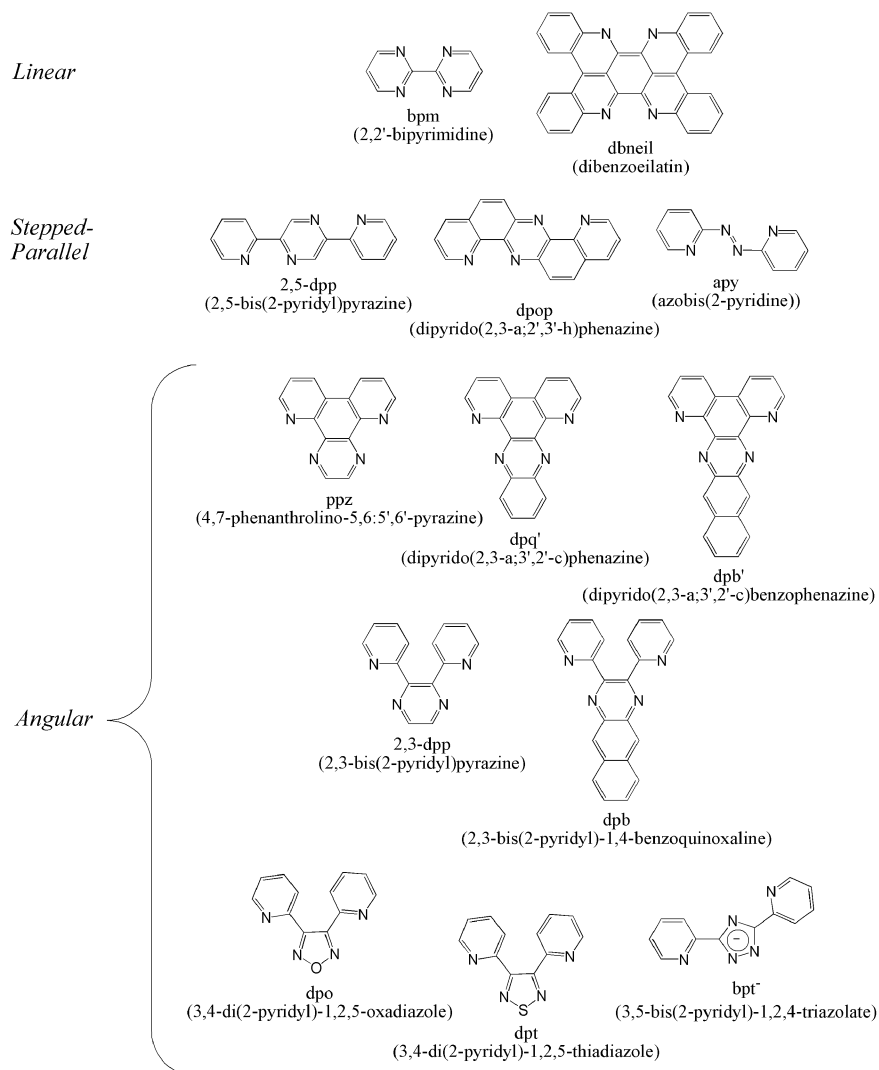


Fig. 4 Polypyridyl bridging ligands.

Electronic and structural consequences of bridging ligand modification

By the systematic variation in the energy of the lowest unoccupied molecular orbital (LUMO) of the bridging ligands, the change in the degree of electronic delocalization (H_{ab}) on the IVCT properties may be assessed. The variations in the bridging ligands include the addition of electron-withdrawing phenyl groups fused to the side of the pyrazine ring through the series ppz, dpq', and dpb' or the modification of the heteroatom in dpo and dpt.

The X-ray crystal structures of the dinuclear cations in *meso*-[$\{\text{Ru}(\text{bpy})_2\}_2(\mu\text{-dpb})\](\text{PF}_6)_4 \cdot 5\text{H}_2\text{O}$ and *meso*-[$\{\text{Ru}(\text{bpy})_2\}_2(\mu\text{-dpb})\](\text{ZnCl}_4)_2 \cdot 5\text{H}_2\text{O}$ exhibit significant distortions in the conformations of the bridging ligands, in comparison with the cations in *meso*-[$\{\text{Ru}(\text{bpy})_2\}_2(\mu\text{-dpb}')\](\text{PF}_6)_4 \cdot 2\text{H}_2\text{O} \cdot 2\{(\text{CH}_3)_2\text{CO}\}$ and *meso*-[$\{\text{Ru}(\text{bpy})_2\}_2(\mu\text{-dpq}')\](\text{ZnCl}_4)_2 \cdot 3\text{H}_2\text{O}$ (Fig. 5). The distortions in the former case are dependent on the identity of the counter-ion and are manifested by differences in the IVCT characteristics between the diastereoisomeric forms of the same complex.

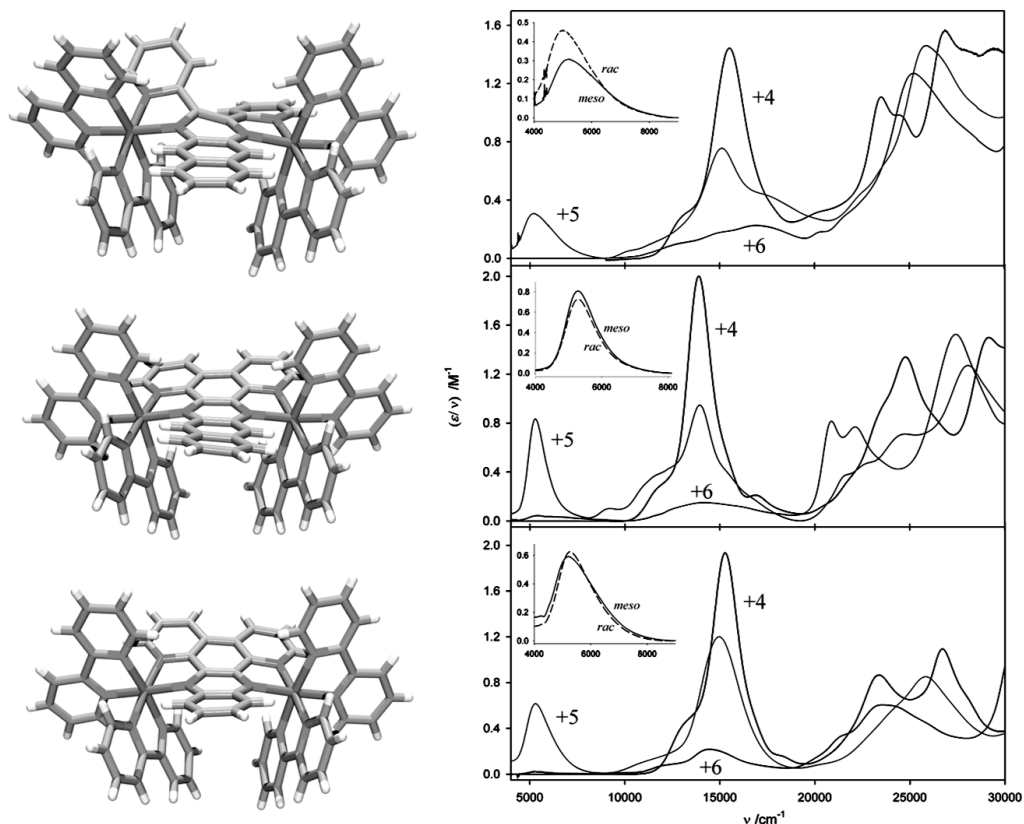


Fig. 5 X-ray crystal structures of *meso*-($\Delta\Delta$)- $[\{\text{Ru}(\text{bpy})_2\}_2(\mu\text{-BL})]^{4+}$ and UV/vis/NIR spectra of *meso*- $[\{\text{Ru}(\text{bpy})_2\}_2(\mu\text{-BL})]^{n+}$ ($n = 4, 5, 6$), BL (top to bottom) = dpb, dpb', and dpq' in 0.1 M $[(n\text{-C}_4\text{H}_9)_4\text{N}]\text{PF}_6/\text{CH}_3\text{CN}$ at -35°C . Insets: overlays of IVCT bands for the *meso* (solid line) and *rac* (dashed line) diastereoisomers.

For all complexes, the IVCT bands are asymmetrically shaped and narrower on the lower energy side (Fig. 5). The electronic coupling parameters, H_{ab} , were determined from eq. 3, where r_{ab} was equated with the through-space geometrical distance between the metal centers [20]. By comparison with the theoretical bandwidths ($\Delta\nu_{1/2}^\circ$) estimated on the basis of the classical two-state theory [16], the relatively narrow bandwidths observed are indicative of significant electronic communication between the metal centers. The results suggest that all the systems lie close to the localized-to-delocalized transition.

Structural distortions in the bridging ligands contribute a redox asymmetry (ΔE_0) to the electron-transfer barrier which enhances the differences between the IVCT characteristics of the diastereoisomers of the same complex [43–45]. For example, electronic delocalization was reduced for both diastereoisomers of $[\{\text{Ru}(\text{bpy})_2\}_2(\mu\text{-dpb})]^{4+}$ relative to their dpb'- and dpq'-bridged analogs due to bridging ligand distortion (Fig. 5).

From the moment analysis of the bands, the general trend is an increase in the extent of delocalization as BL is varied from dpb' to dpq' to ppz. This observed increase in coupling as the bridging ligand LUMO is destabilized [i.e., as the energy separation between the $\text{Ru}(\text{d}\pi)$ orbital and $\pi^*(\text{BL})$ is increased] is somewhat surprising. The results indicate that delocalization is enhanced for complexes incorporating smaller, less sterically hindered bridging ligands.

Since electronic coupling decreases the *effective* electron-transfer distance relative to the geometrical metal-metal separation (which is equated with r_{ab} in eq. 3), the H_{ab} values calculated from this

equation represent lower limits for the electronic coupling parameter. A reevaluation of the *effective* electron-transfer distance from Stark effect spectroscopy [46] revealed that the H_{ab} values are likely to lie closer to the values calculated in the fully delocalized limit [47].

Redox asymmetry contributions in the diastereoisomers of unsymmetrical mixed-valence complexes

The degree of delocalization in the symmetrical complexes $[\{\text{Ru}(\text{bpy})_2\}_2(\mu\text{-dpb'})]^{5+}$ and $[\{\text{Ru}(\text{bpy})_2\}_2(\mu\text{-dpb})]^{5+}$ is diminished by the substitution of the terminal bpy ligands at one end of the complex. The results of a classical analysis for the series of complexes $[\{\text{Ru}(\text{bpy})_2\}(\mu\text{-BL})\{\text{Ru}(\text{pp})_2\}]^{5+}$ (BL = dpb', dpb; pp = bpy, Me₂bpy = 4,4'-dimethyl-2,2'-bipyridine, Me₄bpy = 4,4',5,5'-tetramethyl-2,2'-bipyridine) according to the electrochemical method proposed by Curtis [48] indicate that a greater degree of ground-state delocalization exists in the complexes incorporating the bridging ligand dpb' compared with the dpb analog. The trends in the spectral parameters obtained from the classical analysis reveal that the introduction of redox asymmetry has profound effects: the IVCT bands shift to higher energies, broaden, and decrease in intensity [49]. The onset of localization is accompanied by a significant decrease in H_{ab} , and an increase in λ [26]. The findings reinforce the contention by Reimers and Hush [30] that the accurate treatment of mixed-valence systems in the localized-to-delocalized regime requires a sophisticated model incorporating both symmetric and anti-symmetric modes in which λ and H_{ab} are permitted to vary with ΔE_0 .

IVCT solvatochromism, thermochromism, and ion-pairing contributions

Environmental effects such as solvent and anion rearrangement, and the temperature of the medium, constitute critical contributions to the activation barrier to electron transfer through their influence on λ_0 and ΔE_0 [13,15,18,23,24]. An examination of the solvent, temperature, and anion dependencies of the IVCT process in the diastereoisomers of a series of structurally related complexes was shown to provide a means to evaluate the modification of reorganizational effects and redox asymmetries induced by stereochemical and substitutional changes in the complexes.

IVCT solvatochromism studies on the diastereoisomers of $[\{\text{Ru}(\text{bpy})_2\}_2(\mu\text{-BL})]^{5+}$ [BL = dpb, dpb', dpq' (angular) and 2,5-dpp, dpop and apy (stepped-parallel)] reveal that the systems bridged by dpb, dpb', 2,5-dpp, dpop, and apy are solvent delocalized, while a small residual barrier to solvent exists in the diastereoisomers of the dpq'-bridged complex [50,51]. This is consistent with a class II–III classification for the former systems, while the weak solvent dependence of the latter supports a borderline class II to class II–III classification.

Differential ion-pairing interactions with the diastereoisomers—which are a crucial factor in their chromatographic separation [31,32]—were manifested by differences in their IVCT thermochromism in the presence of relatively strongly, PF₆[−], and weakly, {B(C₆F₅)₄}[−], ion-pairing anions (Fig. 6) [44,52,53]. A significant difference between the IVCT energies for the diastereoisomers of $[\{\text{Ru}(\text{bpy})_2\}_2(\mu\text{-dpb})]^{5+}$ is evident in both media due to the inherent stereochemically induced redox asymmetry, which is also dependent on the identity of the counter-ion.

The anion dependence of the IVCT parameters is unexpected on the basis of eq. 1, although ion-pairing effects have been shown to influence IVCT energies and bandwidths for a number of mixed-valence systems [23,54]. The formation of the ion-pair may be regarded as a redox asymmetry contribution, or as a component of the reorganizational energy due to translation of the counter-ion between the donor and acceptor.

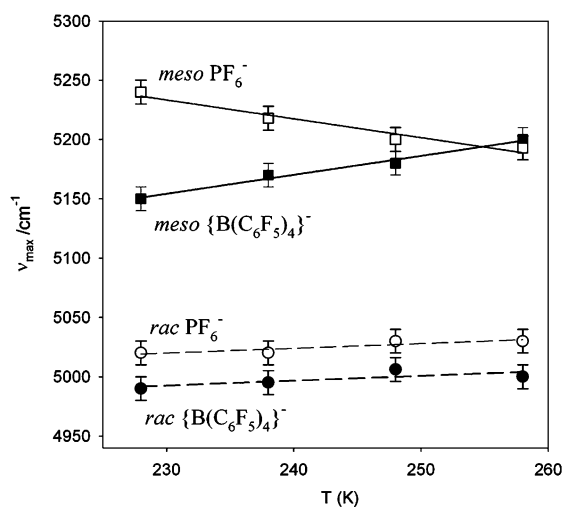


Fig. 6 IVCT thermochromism for *meso* (solid line) and *rac* (dashed line) $[\{\text{Ru}(\text{bpy})_2\}_2(\mu\text{-dpb})]^{5+}$ in 0.1 M $[(n\text{-C}_4\text{H}_9)_4\text{N}]\text{PF}_6$ or 0.02 M $[(n\text{-C}_4\text{H}_9)_4\text{N}]\{\text{B}(\text{C}_6\text{F}_5)_4\}/n\text{-butyronitrile}$.

Dinuclear osmium complexes as probes for spin-orbit coupling ($\Delta E'$) contributions

A complication that has not always been acknowledged in mixed-valence analyses is the existence of multiple IVCT transitions [20]. Due to the effects of ligand field asymmetry and spin-orbit coupling at low-spin $\text{M}^{\text{III}}(\text{d}\pi^5)$ centers ($\text{M} = \text{Fe}, \text{Ru}, \text{Os}$), the t_{2g} orbitals are split into three $\text{d}\pi$ levels (Kramer's doublets) which are linear combinations of the d_{xy} , d_{xz} and d_{yz} atomic orbitals [20,55–58]. In addition to two interconfigurational (IC) transitions, three IVCT transitions arise due to excitation from each of the $\text{M}^{\text{II}}(\text{d}\pi)$ orbitals to the hole at M^{III} . The larger magnitude of the spin-orbit coupling (ξ_{so}) for Os^{III} relative to Ru^{III} and Fe^{III} ($\xi_{\text{so}} \sim 3000$ (Os^{III}), 1000 (Ru^{III}), 800 cm^{-1} (Fe^{III})) [20] typically leads to the observation of a five-band pattern in the IR and NIR regions. The energy splittings between the IC transitions represent the $\Delta E'$ contribution to the intramolecular electron transfer barrier in eq. 1.

The mixed-valence systems $[\{\text{Os}(\text{bpy})_2\}_2(\mu\text{-BL})]^{5+}$ ($\text{BL} = \text{dpb}'$, dpq' , ppz , dpb , 2,3-dpp) are characterized by multiple IVCT and IC bands in the mid-IR and NIR regions [47]. Differences in the relative energies of the IC transitions in the NIR region for the fully oxidized (+6) states, demonstrate that stereochemical effects lead to fundamental changes in the energy levels of the metal-based $\text{d}\pi$ orbitals which are split by spin-orbit coupling and ligand field asymmetry.

Effective electron-transfer distance: Stark effect spectroscopy

While r_{ab} is typically equated with the through-space geometrical distance between the metal centers, the *effective* charge-transfer distance is decreased relative to the geometric distance as electronic coupling across the bridge increases and eqs. 3 and 4 provide a lower limit only for H_{ab} [20]. Electroabsorption (Stark effect) measurements on the IVCT bands of dinuclear mixed-valence complexes have revealed that the actual (adiabatic) charge-transfer distances are often significantly less than the geometric metal–metal distances [46,59–62].

Indeed, Stark effect measurements on the *meso* diastereoisomers of $[\{\text{Ru}(\text{bpy})_2\}_2(\mu\text{-BL})]^{5+}$ ($\text{BL} = \text{dpq}'$, dpb) and $[\{\text{Os}(\text{bpy})_2\}_2(\mu\text{-BL})]^{5+}$ ($\text{BL} = \text{dpb}'$, dpq' , ppz , dpb) reveal that the *effective* electron-transfer distances are a small fraction only of the geometrical metal–metal distances [47,63]. This provides independent support for the classification of the dinuclear ruthenium and osmium complexes as borderline localized-to-delocalized or delocalized systems and contradicts the previous localized assignment for $[\{\text{Os}(\text{bpy})_2\}_2(\mu\text{-BL})]^{5+}$ ($\text{BL} = \text{dpb}$, 2,3-dpp) [64].

EXTENDING THE IVCT PROBE TO TRINUCLEAR POLYMETALLIC ASSEMBLIES

The extension of the IVCT probe to stereochemically pure trinuclear assemblies reveals the contribution of “second-order” interactions due to multiple coupled centers, and provides the link between electron transfer in dinuclear species and in extended arrays and metallosupramolecular systems [65]. While a number of important aspects relating to the influence of the nuclearity and overall oxidation-state polymetallic assemblies on their IVCT properties have been investigated, the majority of studies on the physical characteristics of polymetallic assemblies have been conducted without regard for the inherent stereochemical complexities in such systems [31,32].

Recently, we reported the IVCT properties of the stereochemically pure homo-dinuclear and homo-trinuclear ruthenium complexes *meso*-($\Delta\Delta$)- and *rac*-($\Delta\Delta/\Lambda\Lambda$)-[$\{\text{Ru}(\text{bpy})_2\}_2(\mu\text{-HAT})\}^{4+}$, and *homochiral*-(Δ_3/Λ_3)- and *heterochiral*-($\Delta_2\Lambda/\Lambda_2\Delta$)-[$\{\text{Ru}(\text{bpy})_2\}_3(\mu\text{-HAT})\}^{6+}$ (1,4,5,8,9,12-hexaazatriphenylene) [66,67], shown in Fig. 7.

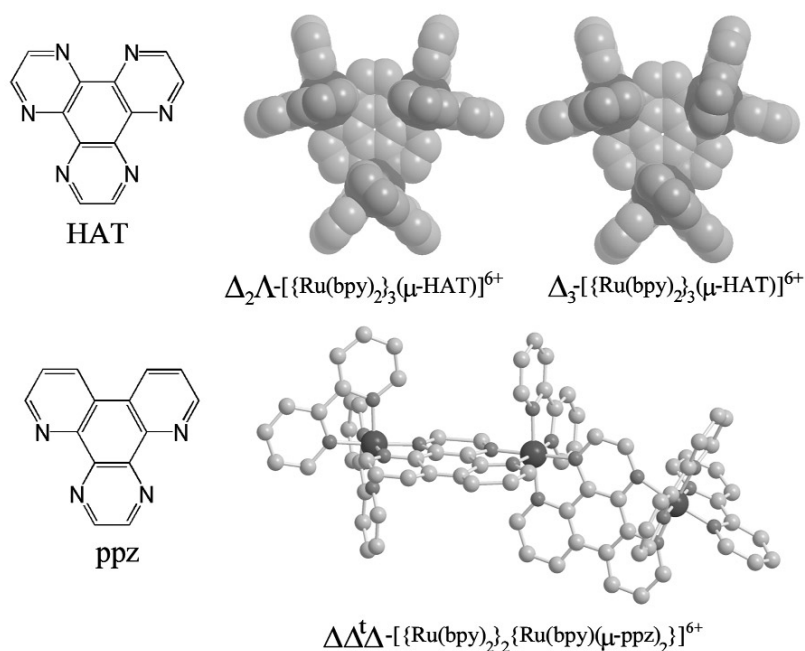


Fig. 7 The bridging ligands HAT and ppz with their corresponding trinuclear complexes.

The dinuclear complexes [$\{\text{Ru}(\text{bpy})_2\}_2(\mu\text{-BL})\}^{5+}$ (HAT and ppz) possess similar electrochemical and IVCT characteristics, which are consistent with their classification as borderline localized-delocalized mixed-valence species. The IVCT characteristics of the singly-oxidized (+7) and doubly oxidized (+8) trinuclear mixed-valence species [$\{\text{Ru}(\text{bpy})_2\}_3(\mu\text{-HAT})\}^{n+}$ [66] and [$\{\text{Ru}(\text{bpy})_2\}_2\{\text{Ru}(\text{bpy})(\mu\text{-ppz})_2\}^{n+}$ ($n = 7, 8$) [68] are markedly different from those of their dinuclear analogs, and vary significantly depending on the extent of oxidation, and the overall geometry of the assembly.

The “cluster-type” system bridged by HAT exhibits significantly greater electronic coupling than the “chain-like” assembly based on ppz. The three ruthenium centers in [$\{\text{Ru}(\text{bpy})_2\}_3(\mu\text{-HAT})\}^{n+}$ are equivalently disposed, and share in the available electron density [66,67]. By comparison, the “chain-like” assembly in $\Delta\Delta^t\Delta$ -[$\{\text{Ru}(\text{bpy})_2\}_2\{\text{Ru}(\text{bpy})(\mu\text{-ppz})_2\}^{n+}$ gives rise to a decreased coupling through the central metal [68]. As a result, the [$\{\text{Ru}(\text{bpy})_2\}_3(\mu\text{-HAT})\}^{6+}$ complex exhibits a comparable degree of electronic coupling to its dinuclear analog, while the degree of electronic coupling in $\Delta\Delta^t\Delta$ -[$\{\text{Ru}(\text{bpy})_2\}_2\{\text{Ru}(\text{bpy})(\mu\text{-ppz})_2\}^{6+}$ is reduced relative to its dinuclear counterpart.

CONCLUSIONS AND FUTURE PROSPECTS

Experimental studies of IVCT in dinuclear mixed-valence complexes have provided crucial insights into the fundamental factors that govern electronic delocalization and the barriers to electron transfer, through the seminal theoretical formalism pioneered by Hush [7,8]. To date, these factors have been probed predominantly by the variation of “global” features of the complexes, such as the identity and coordination environments of the constituent metal centers, or through variations in the macroscopic features of the medium such as the solvent, anions, and temperature. In many cases, the theoretical implications of the results have been confounded by ion-pairing and specific solvation effects, and ambiguities in the geometries of the complexes due to a lack of structural rigidity. In addition, electron-transfer studies on dinuclear polypyridyl complexes of ruthenium and osmium have often neglected their inherent stereochemical identity. Keene and coworkers [31,32] reported the first examples of differences in the photophysical, electrochemical, and spectral properties of the stereoisomers of such systems, although the origins of the stereochemical influences were unclear.

The present study has revealed significant stereochemical effects on the IVCT characteristics of a range of di- and trinuclear mixed-valence complexes. The origins of such influences are attributed to environmental contributions such as specific solvation effects [40], to inherent structural distortions in the bridging ligands [43,44,49] and stereochemically directed anion and solvent interactions [50,51,54]. Within the semi-classical formalism for IVCT, the stereochemical effects are reflected in the Franck–Condon reorganizational contributions to the electron-transfer barrier, the redox asymmetry factor and the spin-orbit coupling term. The latter indicates that these influences modulate the orbital energy levels of the component metal centers themselves [47].

While previous literature reports have elucidated the contributions to IVCT from ion-pairing, specific solvation, and spin-orbit coupling effects, as well as conformational distortions in the bridging ligands [13,15–24], the present observations highlight the subtle effects of such factors on the electron-transfer barrier at the molecular level. In the case of diastereoisomers incorporating rigid bridging ligands, the differences between the forms can be directly related to spatially directed anion and solvent interactions, which also depend on the temperature of the surrounding medium. Complexes incorporating non-rigid bridges pose an additional complexity, as the inherent structural distortion introduces an effective redox asymmetry contribution.

In addition to these fundamental insights, the extension of the IVCT probe to stereochemically pure trinuclear assemblies has revealed the contribution of “second-order” interactions on the IVCT process due to multiple electronically coupled metal centers. Such interactions are enhanced in the presence of strong electronic delocalization, as exemplified by the “cluster-type” systems incorporating the tri-bidentate HAT bridging ligand [66], in contrast to the “chain-like” systems incorporating the closely electronically and structurally related bridging ligand ppz [68].

The elucidation of stereochemical effects on IVCT illustrates the subtle interplay of factors that govern intramolecular electron transfer and electronic delocalization. The findings have significant implications for understanding spatial influences on electron migration in natural systems. At an applied level, stereochemical effects could be exploited in the design of novel molecular materials such as artificial photosynthetic systems for solar energy harvesting.

ACKNOWLEDGMENTS

We gratefully acknowledge the contributions of Prof. Joe Hupp (Northwestern University, USA), Em. Prof. Noel Hush and Prof. Jeff Reimers (University of Sydney, Australia), Prof. Peter Steel (University of Canterbury, N.Z.), Prof. Peter Junk (Monash University, Australia), and Dr. Murray Davies (James Cook University). This work was supported by the Australian Research Council and James Cook University.

REFERENCES

1. G. C. Allen, N. S. Hush. *Prog. Inorg. Chem.* **8**, 357 (1967).
2. M. B. Robin, P. Day. *Adv. Inorg. Chem. Radiochem.* **10**, 247 (1967).
3. J. R. Reimers, N. S. Hush. *J. Am. Chem. Soc.* **126**, 4123 (2004).
4. A. Juris, S. Campagna, I. Bidd, J.-M. Lehn, R. Ziessel. *Inorg. Chem.* **27**, 4007 (1988).
5. T. J. Meyer. *Acc. Chem. Res.* **22**, 163 (1989).
6. V. Balzani, L. De Cola. *Supramolecular Chemistry*, p. 450, Kluwer Academic, Dordrecht (1992).
7. N. S. Hush. *Prog. Inorg. Chem.* **8**, 391 (1967).
8. N. S. Hush. *Electrochim. Acta* **13**, 1005 (1968).
9. C. Creutz, M. D. Newton, N. Sutin. *J. Photochem.* **82**, 47 (1994).
10. R. J. Cave, M. D. Newton. *Chem. Phys. Lett.* **249**, 15 (1996).
11. R. A. Marcus. *J. Chem. Phys.* **26**, 867 (1957).
12. R. A. Marcus. *J. Chem. Phys.* **24**, 966 (1956).
13. C. Creutz. *Prog. Inorg. Chem.* **30**, 1 (1983).
14. C. Creutz, M. H. Chou. *Inorg. Chem.* **26**, 2995 (1987).
15. R. J. Crutchley. *Adv. Inorg. Chem.* **41**, 273 (1994).
16. N. S. Hush. *Coord. Chem. Rev.* **64**, 135 (1985).
17. K. Kalyanasundaram, M. K. Nazeeruddin. *Inorg. Chim. Acta* **226**, 213 (1994).
18. M. D. Ward. *Chem. Soc. Rev.* **24**, 121 (1995).
19. P. F. Barbara, T. J. Meyer, M. A. Ratner. *J. Phys. Chem.* **100**, 13148 (1996).
20. K. D. Demadis, C. M. Hartshorn, T. J. Meyer. *Chem. Rev.* **101**, 2655 (2001).
21. J.-P. Launay. *Chem. Soc. Rev.* **30**, 386 (2001).
22. W. Kaim, A. Klein, M. Glöckle. *Acc. Chem. Res.* **33**, 755 (2000).
23. P. Chen, T. J. Meyer. *Chem. Rev.* **98**, 1439 (1998).
24. D. M. D'Alessandro, F. R. Keene. *Chem. Soc. Rev.* **35**, 424 (2006).
25. S. F. Nelsen. *Chem. Eur. J.* **6**, 581 (2000).
26. B. S. Brunshwig, C. Creutz, N. Sutin. *Chem. Soc. Rev.* **31**, 168 (2002).
27. C. Lambert, G. Nöll. *J. Am. Chem. Soc.* **121**, 8434 (1999).
28. C. Creutz, H. Taube. *J. Am. Chem. Soc.* **91**, 3988 (1969).
29. C. Creutz, H. Taube. *J. Am. Chem. Soc.* **95**, 1086 (1973).
30. J. R. Reimers, N. S. Hush. *Chem. Phys.* **208**, 177 (1996).
31. F. R. Keene. *Coord. Chem. Rev.* **166**, 122 (1997).
32. F. R. Keene. *Chem. Soc. Rev.* **27**, 185 (1998).
33. A. von Zelewsky. *Stereochemistry of Coordination Compounds*, p. 234, John Wiley, Chichester (1995).
34. V. Balzani, A. Juris, M. Venturi, S. Campagna, S. Serroni. *Chem. Rev.* **96**, 759 (1996).
35. L. S. Kelso, D. A. Reitsma, F. R. Keene. *Inorg. Chem.* **35**, 5144 (1996).
36. T. J. Rutherford, F. R. Keene. *Inorg. Chem.* **36**, 2872 (1997).
37. T. J. Rutherford, O. Van Gijte, A. Kirsch-De Mesmaeker, F. R. Keene. *Inorg. Chem.* **36**, 4465 (1997).
38. J. A. Treadway, P. Chen, T. J. Rutherford, F. R. Keene, T. J. Meyer. *J. Phys. Chem. A* **101**, 6824 (1997).
39. V. Gutmann. *Electrochim. Acta* **21**, 661 (1976).
40. D. M. D'Alessandro, F. R. Keene. *Chem. Phys.* **324**, 8 (2006).
41. S. D. Bergman, I. Goldberg, A. Barbieri, F. Barigelletti, M. Kol. *Inorg. Chem.* **43**, 2355 (2004).
42. D. M. D'Alessandro, F. R. Keene, S. D. Bergman, M. Kol. *Dalton Trans.* 332 (2005).
43. D. M. D'Alessandro, L. S. Kelso, F. R. Keene. *Inorg. Chem.* **40**, 6841 (2001).
44. D. M. D'Alessandro, P. C. Junk, F. R. Keene. *Supramol. Chem.* **17**, 529 (2005).

45. C. Richardson, P. J. Steel, D. M. D'Alessandro, P. C. Junk, F. R. Keene. *J. Chem. Soc., Dalton Trans.* 2775 (2002).
46. G. U. Bublitz, S. G. Boxer. *Annu. Rev. Phys. Chem.* **48**, 213 (1997).
47. D. M. D'Alessandro, P. H. Dinolfo, M. S. Davies, J. T. Hupp, F. R. Keene. *Inorg. Chem.* **45**, 3261 (2006).
48. J. C. Curtis, J. S. Bernstein, R. H. Schmehl, T. J. Meyer. *Chem. Phys. Lett.* **81**, 48 (1981).
49. D. M. D'Alessandro, F. R. Keene. *Aust. J. Chem.* **58**, 767 (2005).
50. D. M. D'Alessandro, A. C. Topley, M. S. Davies, F. R. Keene. *Chem. Eur. J.* **12**, 4873 (2006).
51. D. M. D'Alessandro, F. R. Keene. *New J. Chem.* **30** (2), 228 (2006).
52. D. M. D'Alessandro, F. R. Keene. *Dalton Trans.* 3950 (2004).
53. D. M. D'Alessandro, F. M. Foley, M. S. Davies, P. C. Junk, F. R. Keene. *Polyhedron* **26**, 216 (2007).
54. E. A. Fellows, F. R. Keene. *J. Phys. Chem. B* **111**, 6667 (2007).
55. E. M. Kober, T. J. Meyer. *Inorg. Chem.* **21**, 3967 (1982).
56. E. M. Kober, K. A. Goldsby, D. N. S. Narayana, T. J. Meyer. *J. Am. Chem. Soc.* **105**, 4303 (1983).
57. E. M. Kober, T. J. Meyer. *Inorg. Chem.* **22**, 1614 (1983).
58. G. Neyhart. PhD thesis, p. 445, University of North Carolina, Chapel Hill (1988).
59. B. S. Brunschwig, C. Creutz, N. Sutin. *Coord. Chem. Rev.* **177**, 61 (1998).
60. K. A. Walters. In *Comprehensive Coordination Chemistry II*, J. A. McCleverty, T. J. Meyer (Ed.), pp. 303–313, Elsevier, Oxford (2003).
61. A. Ferretti. *Coord. Chem. Rev.* **238–239**, 127 (2003).
62. F. W. Vance, R. D. Williams, J. T. Hupp. *Int. Rev. Phys. Chem.* **17**, 307 (1998).
63. D. M. D'Alessandro, P. H. Dinolfo, J. T. Hupp, P. C. Junk, F. R. Keene. *Eur. J. Inorg. Chem.* 772 (2006).
64. M. M. Richter, K. J. Brewer. *Inorg. Chem.* **32**, 2827 (1993).
65. D. M. D'Alessandro, F. R. Keene. *Chem. Rev.* **106**, 2270 (2006).
66. D. M. D'Alessandro, F. R. Keene. *Chem. Eur. J.* **11**, 3679 (2005).
67. D. M. D'Alessandro, M. S. Davies, F. R. Keene. *Inorg. Chem.* **45**, 1656 (2006).
68. D. M. D'Alessandro, F. Richard Keene. *Dalton Trans.* 1060 (2006).